J. Phys. A: Math. Theor. **45** (2012) 085209 (18pp) doi:10.1088/1751-8113/45/8/085209

Nodal domains of a non-separable problem—the right-angled isosceles triangle

Amit Aronovitch[1], **Ram Band**[1,2], **David Fajman**[3] **and Sven Gnutzmann**[4]

[1] Department of Physics of Complex Systems, The Weizmann Institute of Science, 76100 Rehovot, Israel
[2] School of Mathematics, University of Bristol, Bristol BS8 1TW, UK
[3] Max Planck Institute for Gravitational Physics (Albert Einstein Institute), Am Mühlenberg 1, D-14476 Golm, Germany
[4] School of Mathematical Sciences, University of Nottingham, University Park, Nottingham NG7 2RD, UK

E-mail: aronovitch@gmail.com, rami.band@bristol.ac.uk, David.Fajman@aei.mpg.de and Sven.Gnutzmann@nottingham.ac.uk

Received 7 October 2011, in final form 14 January 2012
Published 14 February 2012
Online at stacks.iop.org/JPhysA/45/085209

Abstract
We study the nodal set of eigenfunctions of the Laplace operator on the right-angled isosceles triangle. A local analysis of the nodal pattern provides an algorithm for computing the number ν_n of nodal domains for any eigenfunction. In addition, an exact recursive formula for the number of nodal domains is found to reproduce all existing data. Eventually, we use the recursion formula to analyse a large sequence of nodal counts statistically. Our analysis shows that the distribution of nodal counts for this triangular shape has a much richer structure than the known cases of regular separable shapes or completely irregular shapes. Furthermore, we demonstrate that the nodal count sequence contains information about the periodic orbits of the corresponding classical ray dynamics.

PACS numbers: 03.65.Ge, 03.65.Sq, 05.45.Mt
Mathematics Subject Classification: 35Pxx, 58C40, 58J50

(Some figures may appear in colour only in the online journal)

1. Introduction

More than 200 years ago Chladni pioneered the study of standing waves with his experiments on sound figures for the vibration modes of plates [1]. The sound figures revealed that one may characterize the modes by looking at the nodal set—the lines on the plate which do not take part in the vibration and which are visualized in a sound figure. For each mode he drew the nodal pattern and counted the number of nodal lines and nodal domains. With his work he not only laid the foundations of modern acoustics but also started a thread in theoretical and mathematical physics which lead to such classic results as Sturm's oscillation theorem [2] and which continues to this day.

The mathematical framework starts with the Laplacian Δ on a compact Riemannian manifold $\mathcal{M}$—for the purpose of this paper it will be sufficient to consider dimension 2. If the manifold has a boundary, then Dirichlet boundary conditions will be assumed. One studies the eigenvalue problem

$$-\Delta\varphi = \lambda\varphi, \qquad \varphi|_{\partial\mathcal{M}} = 0. \tag{1.1}$$

The solutions define the discrete spectrum of (non-negative) eigenvalues $\{\lambda_N\}_{N=1}^{\infty}$ which we assume to be ordered as $0 \leqslant \lambda_1 \leqslant \lambda_2 \leqslant \cdots$. The corresponding eigenfunctions will be denoted φ_N. A nodal domain of the eigenfunction φ_N is a connected region in $\mathcal{M}$ where the sign of φ_N does not change. We define the nodal count ν_N as the number of nodal domains in φ_N. The nodal counts $\{\nu_N\}$ form a sequence of integer numbers which characterizes the vibration modes φ_N of the shape $\mathcal{M}$. In the case of degeneracies in the spectrum the nodal count is not uniquely defined. This may be overcome in various ways, e.g. by fixing a basis (and an order in each degeneracy class). Some results on nodal counts are valid for any choice for the basis of eigenfunctions—a famous example is the classic theorem by Courant [3] which states $\nu_N \leqslant N$.

More recently, it has been proposed [4] that one may use the nodal count sequence to distinguish between the following: (i) regular shapes where the Laplacian is separable and the corresponding ray (billiard) dynamics is integrable, and (ii) irregular shapes where the ray dynamics is completely chaotic (see also [5–9]).

In the regular separable case the nodal set has a checker board pattern with crossing nodal lines. The nodal count can easily be found using Sturm's oscillation theorem in both variables. In this case many properties of the nodal count sequence can be developed analytically—e.g. the statistical distribution of the scaled nodal count $\xi_N = \nu_N/N$ can be described by an explicit limiting function $P(\xi)$. This function has some generic universal features: $P(\xi)$ is an increasing function with support $0 \leqslant \xi \leqslant \xi_{\text{crit}} < 1$, where ξ_{crit} is a system-dependent cut-off. Near the cut-off, for $\xi < \xi_{\text{crit}}$ the distribution behaves as $P(\xi) \propto (\xi_{\text{crit}} - \xi)^{-1/2}$.

In the irregular case, no explicit counting functional is known. In this case, the nodal lines generally do not have any intersections and counting nodal domains rely on numerical algorithms (such as the Hoshen–Kopelman algorithm [10]) that represent the eigenfunctions on a grid of finite resolution. The numerical procedure is reliable if the resolution is high enough to resolve the distance between nodal lines near avoided intersections [11]. For high lying eigenvalues λ_N, the algorithm is time-consuming due to the increasing grid size. The numerical experiments have shown that a limiting distribution $P(\xi)$ takes the form $P(\xi) = \delta(\xi - \overline{\xi})$, where $\overline{\xi}$ is a universal constant (i.e. it does not depend on the shape). This and other numerical findings have been shown to be consistent with a seminal conjecture by Berry [12] which states that the statistics of eigenfunctions for an irregular (chaotic) shape can be modelled by the Gaussian random wave (a superposition of planar waves with the same wavelengths, random direction and random phase). Bogomolny and Schmit [13] realized that the nodal structure of a two-dimensional random wave may be modelled by a parameter-free critical percolation model (see also [14, 15]). With this heuristic model they were able to derive an explicit value for $\overline{\xi}$ (and other features of the nodal set) with excellent agreement to all numerical data. One interesting implication of the critical percolation model is that nodal lines can be described by SLE which has been checked affirmatively in numerical experiments [16–18]. Meanwhile, some features of the nodal count have been proven rigorously for random waves on a sphere [19]—these rigorous results imply the δ-type distribution for $P(\xi)$ (but cannot predict the value $\overline{\xi}$).

Another interesting applications of the nodal count that we will touch in this paper are inverse questions. Two inverse questions have been discussed in some detail: (i) can one

resolve isospectrality by looking at the additional information contained in the nodal count [20–22]; and (ii) can one count the shape of a drum [23–26]? In other words, does the sequence of nodal counts (ordered by increasing eigenvalues) determine the shape of the manifold $\mathcal{M}$? We refer to the shape rather than the manifold itself as the nodal counts are invariant under scaling of $\mathcal{M}$.

Both inverse questions have been answered in the affirmative for certain sets of shapes and some cases have been proven rigorously [21, 26]. However, most recently the first example of a pair of non-isometric manifolds with identical nodal sequences was found [22].

In some cases it could be shown that the geometrical information is stored in the nodal sequence in a way which is very similar to the way it is stored in spectral functions. For instance, the nodal count sequence for regular shapes with a separable Laplacian can be described by a semiclassical trace formula [23–25]. This trace formula is very similar to the known trace formulas for spectral functions—it is a sum over periodic orbits (closed ray trajectories) on the manifold where each term contains geometric information about the orbit. It has been shown that this trace formula can be used to count the shape of a surface of revolution [25].

In the irregular case, the existence of a trace formula is an open question (unpublished numerical experiments by the authors give some support to the existence of such a formula).

In this work, we continue the thread of research summarized above and consider the nodal set of the eigenfunctions of one particular shape: the right-angled isosceles triangle (i.e. the triangle with angles 45°–45°–90°). While this shape is regular with an integrable ray dynamics, the Laplacian is not separable.

Our main result is an explicit algorithm for the nodal counts. In contrast to the numerical algorithm used for irregular shapes, our algorithm is exact and does not rely on a finite resolution representation of the wavefunction. Although the algorithm is specific to this shape, the approach may serve as the first step to generalize explicit formulas for nodal counts beyond the separable case where very few results are currently available. Furthermore, we conjecture a recursion formula that allows very efficient evaluation of nodal counts for high eigenvalues.

In the remainder of the introduction, we will introduce the spectrum and the basis of eigenfunctions for the right-angled isosceles triangle. In section 2, we will discuss the nodal structure of the eigenfunctions and state the nodal count algorithm and the recursion formula as our main results. In section 3, we apply the nodal count algorithm to compute the distribution $P(\xi)$ of scaled nodal counts and discuss the consistency of the observed nodal counts with the existence of a trace formula.

1.1. Eigenvalues and eigenfunctions of the Laplacian for the right-angled isosceles triangle

Let $\mathcal{D} \subset \mathbb{R}^2$ be the right-angled isosceles triangle of area $\pi^2/2$. For definiteness, we choose the triangle as

$$\mathcal{D} = \{(x, y) \in [0, \pi]^2 : \ y \leqslant x\}.$$

The eigenvalue problem is stated by

$$-\Delta\varphi(x, y) = -\left(\partial_x^2 + \partial_y^2\right)\varphi(x, y) = \lambda\varphi(x, y) \quad \text{with } \varphi(x, y)|_{\partial\mathcal{D}} = 0.$$

The spectrum of eigenvalues is given by

$$\lambda_{m,n} = m^2 + n^2 \quad \text{for} \quad m,\ n \in \mathbb{N}^* \text{ and } m > n$$

and the corresponding eigenfunctions

$$\varphi_{m,n}(x, y) = \sin(mx)\sin(ny) - \sin(nx)\sin(my) \tag{1.2}$$

form a complete orthogonal basis.

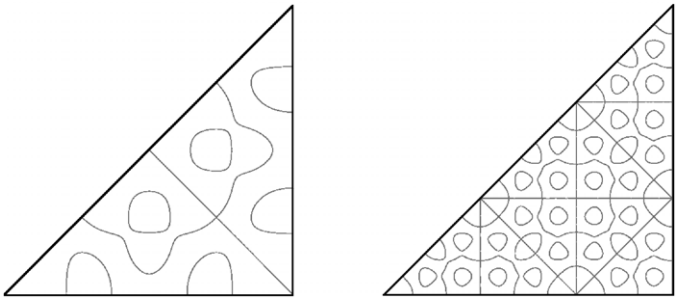

Figure 1. Two examples for the tiling cases: (*a*) $\varphi_{9,5}$ and (*b*) $\varphi_{21,6}$.

We denote the nodal count (the number of nodal domains) for $\varphi_{m,n}(x, y)$ by $\nu_{m,n}$. Let us order the spectrum in increasing order, written as a sequence $\{\lambda_N\}_{N=1}^{\infty}$, such that $\lambda_N \leqslant \lambda_{N+1}$. Here, $N \equiv N_{m,n}$ is an integer function of the integers m and n (we will continue to suppress the reference to m and n), and we have mildly abused the notation by writing $\lambda_N = \lambda_{N_{m,n}} = \lambda_{m,n}$. The spectrum contains degeneracies of a number-theoretic flavour. For a g-fold degenerate eigenvalue $\lambda_N = \lambda_{N+1} = \cdots = \lambda_{N+g-1}$, we define $N_{m,n}$ by ordering the degenerate values by increasing n. This ordering is arbitrary and has been chosen for definiteness—none of our results here would change with a different choice.

In principle, one may also be interested in the nodal patterns of arbitrary eigenfunctions in a degeneracy class. Indeed, many physical applications may imply that the basis functions $\varphi_{m,n}$ cannot be regarded as typical as soon as one looks at a degenerate eigenvalue. However, in this paper we will focus exclusively on the nodal counts of the basis functions $\varphi_{m,n}$—for two reasons: (i) understanding the nodal patterns of arbitrary superpositions of the basis functions $\varphi_{m,n}$ is a much harder problem which does not follow naturally from understanding just the basis; and (ii) this choice of basis is natural for any computations.

2. The nodal pattern

This section describes the main properties of the nodal pattern of the eigenfunctions φ_{mn}. These observations are then used in subsection 2.3 to infer an exact algorithm for counting nodal domains in the triangle. Eventually, we propose a very efficient recursion formula for the nodal counts of the eigenfunctions φ_{mn} in subsection 2.5.

2.1. A tiling structure of the nodal lines

The eigenvalue problem on the triangle possesses some symmetry properties which are revealed in the nodal pattern of the eigenfunctions, $\varphi_{m,n}$. Specifically, there are eigenfunctions whose nodal sets show a tiling structure.

(1) For $m > n$ with $(m+n) \mod 2 = 0$, the eigenfunction $\varphi_{m,n}$ is an antisymmetric function with respect to the line $y = \pi - x$. This line is therefore part of the nodal set of $\varphi_{m,n}$. The complementary nodal set decomposes into two isometric patterns, each from either side of the line. Each of these two patterns is similar to the nodal set pattern of the eigenfunction $\varphi_{m',n'}$ with $m' = (m+n)/2$ and $n' = (m-n)/2$ (figure 1(*a*)).

(2) For $m > n$ with $\gcd(m, n) = d > 1$, the nodal set of the eigenfunction $\varphi_{m,n}$ consists of d^2 identical nodal patterns. Each of these patterns is contained within a subtriangle and

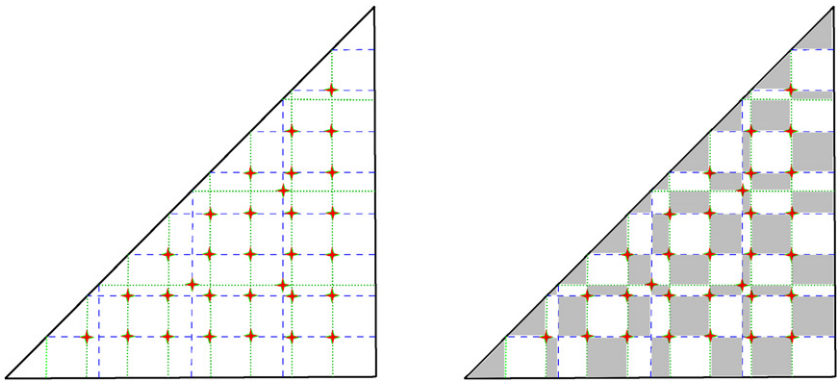

Figure 2. (*a*) The nodal sets $N^1_{9,4}$ (dotted lines) and $N^2_{9,4}$ (dashed lines). (*b*) The subdomains where $\varphi^1_{9,4}$ and $\varphi^2_{9,4}$ have the same sign.

they are tiled together to form the complete pattern. Each such subpattern is similar to the nodal set of the eigenfunction $\varphi_{m',n'}$ for $m' = m/d$ and $n' = n/d$ (figure 1(*b*)).

The observations above follow directly from (1.2).

2.2. *Characterization of the nodal set*

Let us now characterize the nodal set of the eigenfunction $\varphi_{m,n}$. We assume that the nodal set of $\varphi_{m,n}$ does not have the tiling behaviour described in section 2.1, i.e. $\gcd(m, n) = (m + n) \bmod 2 = 1$. Otherwise, one may reduce the values of m, n, as described above, to a smaller pair m', n', which does satisfy this condition, and study the nodal set of $\varphi_{m',n'}$ within the reduced triangle. In particular, it is proved in lemma A.1 in the appendix that for m, n which satisfy the condition above, the nodal lines of the eigenfunction $\varphi_{m,n}$ do not cross. This observation is used below to characterize the nodal set.

We write the eigenfunction $\varphi_{m,n}$ as the difference of the following two functions:

$$\varphi^1_{m,n}(x, y) = \sin(mx)\sin(ny),$$
$$\varphi^2_{m,n}(x, y) = \sin(nx)\sin(my).$$

Their nodal sets are correspondingly

$$N^1_{m,n} = \left\{(x, y) \in \mathcal{D} \middle| x \in \frac{\pi}{m}\mathbb{N} \vee y \in \frac{\pi}{n}\mathbb{N}\right\},$$
$$N^2_{m,n} = \left\{(x, y) \in \mathcal{D} \middle| x \in \frac{\pi}{n}\mathbb{N} \vee y \in \frac{\pi}{m}\mathbb{N}\right\}.$$

These are regular checkerboard patterns whose nodal domains are open rectangles and triangles (figure 2(*a*)).

The intersection $N^1_{m,n} \cap N^2_{m,n}$ is the set of points

$$V_{m,n} = \left\{\frac{\pi}{m}(i, j) \,|0 < j < i < m\right\} \cup \left\{\frac{\pi}{n}(i, j) \,|0 < j < i < n\right\}$$

(marked with stars in figure 2). The eigenfunction φ_{mn} vanishes at these points. Hence, nodal lines pass through them. In the following, we analyse the run of the nodal lines of φ_{mn} between

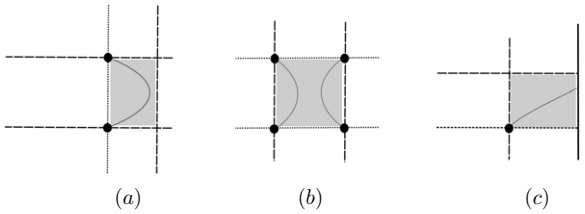

Figure 3. Different cases of connecting $V_{m,n}$ within the shaded sub-domains. (a) A rectangle with two points from $V_{m,n}$. (b) A rectangle with four points from $V_{m,n}$. (c) A rectangle with a single point from $V_{m,n}$.

the points of the set $V_{m,n}$. The union $N^1_{m,n} \cup N^2_{m,n}$ divides $\mathcal{D}$ into cells shaped as rectangles and triangles of various sizes. These cells are the connected components of $\mathcal{D}\setminus\left(N^1_{m,n} \cup N^2_{m,n}\right)$. The nodal set of φ_{mn} is contained within the cells in which $\varphi^1_{m,n}$ and $\varphi^2_{m,n}$ have the same sign. These cells are interlacing in the checkerboard pattern formed by $N^1_{m,n} \cup N^2_{m,n}$. We call them the *shaded cells* and they appear so in figure 2(b).

The connection between the points in $V_{m,n}$ by nodal lines can be easily determined by going over the shaded cells and distinguishing between the following cases.

(1) A rectangular cell adjacent to two points of $V_{m,n}$. A non-self-intersecting nodal line connects these two points. This is proved in lemma A.2. An example is shown in figure 3(a).
(2) A rectangular cell adjacent to four points of $V_{m,n}$. Two nodal lines connect the two pairs of vertices in either a horizontal or a vertical non-crossing pattern. One can determine whether the pattern is horizontal or vertical by comparing the sign of $\varphi_{m,n}$ at the middle point of the rectangle with the sign of $\varphi_{m,n}$ at one of the neighbouring cells. This is proved in lemma A.2. This lemma also proves that a non-tiling eigenfunction, $\varphi_{m,n}$, cannot vanish at the middle point of the rectangular cell. An example is shown in figure 3(b).
(3) A cell adjacent to a single point of $V_{m,n}$. This happens only for a cell which is adjacent to the boundary of $\mathcal{D}$. The $V_{m,n}$ point is then connected to the boundary of $\mathcal{D}$ by a simple non-intersecting nodal line. This is proved in lemma A.3. An example is shown in figure 3(c).
(4) A triangular cell which does not contain any point of $V_{m,n}$. In this case there is no nodal line which passes through this triangle. This is proved in lemma A.3.

2.3. An algorithm for counting the nodal domains

We now describe an algorithm for counting $\nu_{m,n}$, the number of nodal domains of $\varphi_{m,n}$, based on the observations of the previous section. If the values of m, n correspond to an eigenfunction with a tiling behaviour we replace them by their *reduced values*.

(1) For $m > n$ with $\gcd(m,n) = d > 1$, set the new values of m, n to be $m' = m/d$ and $n' = n/d$. Set the number of tiles to be d^2.
(2) For $m > n$ with $(m+n) \mod 2 = 0$, set the new values of m, n to be $m' = (m+n)/2$ and $n' = (m-n)/2$. Set the number of tiles to be 2.

The number of nodal domains $\nu_{m,n}$ for the original values of m, n equals to the number of tiles times the number of nodal domains of the reduced values. We now proceed, assuming the

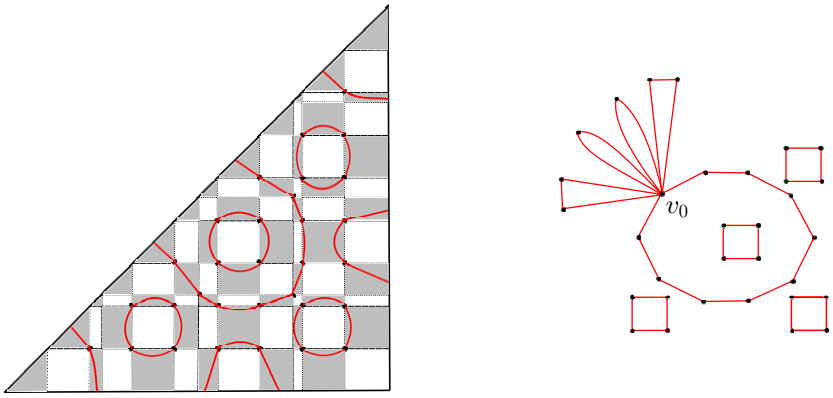

Figure 4. (*a*) The nodal set pattern of $\varphi_{9,4}$. (*b*) The graph $G_{9,4}$ which is produced by the counting algorithm.

values of m, n were reduced. We create a graph, $G_{m,n}$, whose vertices are $V_{m,n}$ with an additional anchor vertex, v_0, which stands for the boundary of the triangle, $\partial\mathcal{D}$. The edges of the graph would stand for the nodal lines which connect the vertices of $V_{m,n}$. We go over all shaded cells as described above and for each of them add either zero, one or two edges to the graph connecting the relevant vertices. The number of vertices in a cell determines their connectivity, as described in the previous section[5]. The cells which contain a nodal line connected to the boundary $\partial\mathcal{D}$, would contribute a single edge to the graph connecting the relevant vertex of $V_{m,n}$ to the vertex v_0. Figure 4 demonstrates the graph $G_{m,n}$ which corresponds to a certain nodal set pattern.

For a planar graph, we define an *interior face* as a finite area two-dimensional domain bounded by the graph's edges. Once the graph $G_{m,n}$ is constructed, the number of nodal domains, $\nu_{m,n}$, is given by the number of the graph's interior faces plus 1. According to Euler's formula for planar graphs, the number of interior faces of $G_{m,n}$ equals $E(G_{m,n}) - |V_{m,n}| + c(G_{m,n})$, where $E\left(G_{m,n}\right)$ is the number of edges of $G_{m,n}$ and $c\left(G_{m,n}\right)$ is the number of its connected components. We, therefore, obtain

$$\nu_{m,n} = 1 + E(G_{m,n}) - |V_{m,n}| + c(G_{m,n}),$$

which completes the algorithm once $c(G_{m,n})$ is calculated ($E(G_{m,n})$ and $|V_{m,n}|$ are known at this stage).

2.4. Boundary intersections and nodal loops

Above we have discussed the nodal count $\nu_{m,n}$. We now introduce two further quantities which reflect the nodal set structure of the eigenfunction $\varphi_{m,n}$. The first is the number of intersections of the nodal set of $\varphi_{m,n}$ with the boundary, $\partial\mathcal{D}$, which we denote by $\eta_{m,n}$ and call *boundary intersections*. The second is the number of nodal lines which neither touch the boundary nor intersect themselves or any other nodal lines. We call those *nodal loops*, and denote their number by $I_{m,n}$. In the case where $\varphi_{m,n}$ does not have a tiling structure, each nodal line is either

[5] In addition, explicitly computing the value of $\varphi_{m,n}$ at a specific point of the cell might be required in the case of a cell adjacent to four vertices.

a loop or a segment connected to the boundary at two points. Hence, the connection between the quantities defined above (in the non-tiling case) is given by the following formula:

$$\nu_{m,n} = 1 + \tfrac{1}{2}\eta_{m,n} + I_{m,n}. \tag{2.1}$$

As an example, in figure 4 one can count $\eta_{9,4} = 10$ and $I_{9,4} = 4$. The algorithm described in the preceding section can be used to count $\eta_{m,n}$ and $I_{m,n}$.

(1) The number of nodal loops, $I_{m,n}$, is given as the number of connected components of the graph $G_{m,n}$ minus 1.
(2) The number of nodal intersections, $\eta_{m,n}$, equals twice the number of independent cycles of the $G_{m,n}$ component which contains v_0.

One can show ([28]) that the number of boundary intersections of the nodal set of φ_{mn} in the non-tiling case is given by

$$\eta_{m,n} = m + n - 3. \tag{2.2}$$

Combining this with (2.1) indicates that any formula for the nodal loop count $I_{m,n}$ would yield a formula for the nodal count $\nu_{m,n}$ and vice versa.

2.5. A recursive formula for the nodal loop count

In subsection 2.3, we have described an exact algorithm that allowed us to compute the nodal loops count. By direct inspection of tables of evaluated loop counts, we have noticed strong correlations between the counts of different eigenfunctions. An extensive analysis of such tables allowed us to infer a recursive formula that we will now describe. Apart from regenerating all data that we looked at explicitly, we have checked that the empirical formula correctly predicts all loop counts for the first 100 000 non-tiling eigenfunctions (this assures agreement of the nodal counts at least up to $N = 246\,062$, i.e. for all $\varphi_{m,n}$ with $m^2 + n^2 \leqslant 628\,325$).

We propose that the loop count $I_{m,n}$ is given by

$$I_{m,n} = \tilde{I}\big(n, \tfrac{1}{2}(m - n - 1), 0\big),$$

where the three parameter function $\tilde{I}(n, k \text{ and } l)$ is defined by the following recursive formula:

$$\tilde{I}(n,k,l) := \begin{cases} 0 & n = 1 \text{ or } k = 0 \\ \left\lfloor \dfrac{n}{2k+1} \right\rfloor \left(lk + (2l+1)\,k^2\right) + \tilde{I}(n \bmod (2k+1),\ k,\ l) & 2k+1 < n \\ \dfrac{1}{2}\left\lfloor \dfrac{k}{n} \right\rfloor (2l+1)\left(n^2 - n\right) + \tilde{I}(n,\ k \bmod n,\ l) & 2k+1 > 2n \\ \left(l + \dfrac{1}{2}\right)(2k^2 + n^2 - n - 2nk + k) + \dfrac{1}{2}k + \tilde{I}(2k - n + 1, n - k - 1, l + 1) & n < 2k+1 < 2n. \end{cases} \tag{2.3}$$

As usual we have assumed that m and n correspond to a non-tiling case (otherwise, the reduction as described above should be made).

Remarks

(1) Note that the description of (2.3) in terms of the parameters $(n, k) = \big(n, \frac{1}{2}(m - n - 1)\big)$ is more compact than a description in terms of the original parameters m and n.
(2) If the initial values of parameters, n and k correspond to a non-tiling case, i.e. $\gcd(n + 2k + 1, n) = 1$, then this condition will hold for all recursive applications of the formula.

(3) One can verify that recursive applications of the formula terminate at some stage. Namely, that during the recursive applications we arrive at either $n = 1$ or $k = 0$.

3. Applications to the nodal counting sequence

3.1. The nodal count distribution

Let us now discuss the asymptotic statistics of the number of nodal domains in terms of the nodal count distribution. In section 1.1, we have given a definition of the nodal count sequence $\{\nu_N\}_{N=1}^{\infty}$. Let ν_N be the nodal count of the Nth eigenfunction. From Courant's nodal domain theorem [3], we know that $\nu_N \leqslant N$. While the Courant bound is only realized by a finite number of eigenfunctions [27], one may still expect that the nodal count will grow $\nu_N \sim N$ with the index N. It thus makes sense to introduce the scaled nodal count

$$\xi_N = \frac{\nu_N}{N} \tag{3.1}$$

and ask about the asymptotic behaviour of ξ_N as $N \to \infty$. The latter has been explored by Blum *et al* [4] for general two-dimensional billiards in terms of the nodal count distribution in the interval $\lambda \leqslant \lambda_N \leqslant \lambda(1+g)$ for large λ. The parameter $g > 0$ defines the width of the interval. The limiting distribution is defined as

$$P_{\lambda,g}(\xi) = \frac{1}{N(\lambda, g)} \sum_{N:\lambda_N \in [\lambda,(1+g)\lambda]} \delta_\epsilon(\xi - \xi_N), \tag{3.2}$$

where $\delta_\epsilon(x) = \epsilon \left(\pi (x^2 + \epsilon^2)\right)^{-1}$ is a regularized delta-function (the limit $\epsilon \to 0$ will always be implied in the following) and $N(\lambda, g)$ is the number of eigenfunctions in the interval. The integrated distribution will be denoted by

$$I_{\lambda,g}(\xi) = \int_0^{\xi} P_{\lambda,g,\epsilon}(\xi')\, \mathrm{d}\xi'. \tag{3.3}$$

As mentioned in the introduction, an explicit formula for the limiting distribution

$$P(\xi) = \lim_{\lambda\to\infty} P_{\lambda,g}(\xi) \tag{3.4}$$

can be derived for separable Laplacians using semiclassical methods [4], while for irregular (chaotic) shapes Bogomolny's percolation model [13] predicts that the limiting distribution is concentrated at a universal value $\overline{\xi}$ which is consistent with all numerical data available. The right-angled isosceles triangle is neither an irregular shape (in fact the ray dynamics is integrable) nor are its wavefunctions separable. The proposed recursion formula (2.3) allows us to find the nodal counts for large sequences of eigenfunctions very efficiently on a computer. We calculated the nodal counts for all eigenfunctions with $\sqrt{\lambda_N} \leqslant 13\,000$ (about 66 million eigenfunctions) and extracted the nodal count distributions in various intervals. In the remainder of this section, we will set $g = 1$ and discuss the numerical results.

Figure 5 reveals that the nodal count distribution $P_{\lambda,1}(\xi)$ (with $\lambda = 9000^2$) for the isosceles triangle contains a lot of puzzling structure that neither resembles the monotonic behaviour known from separable billiards nor the single delta-peak known to describe chaotic billiards. Instead, the distribution consists of many peaks whose strengths and distances form a visible pattern. Each peak apparently has a further substructure. The same structure appears if one only includes wavefunctions without tiling behaviour (or with a specific number of tiles).
Comparing the nodal count distributions $P_{\lambda,1}(\xi)$ for various values of λ gives us some insight into the asymptotic behaviour of $P_{\lambda,1}(\xi)$. Figure 6 shows how two peaks in the distribution move and change shape as λ increases: all peaks move to the left and become sharper. The comparison reveals that our numerical calculation of $P(\xi)$ has not converged—in spite of the

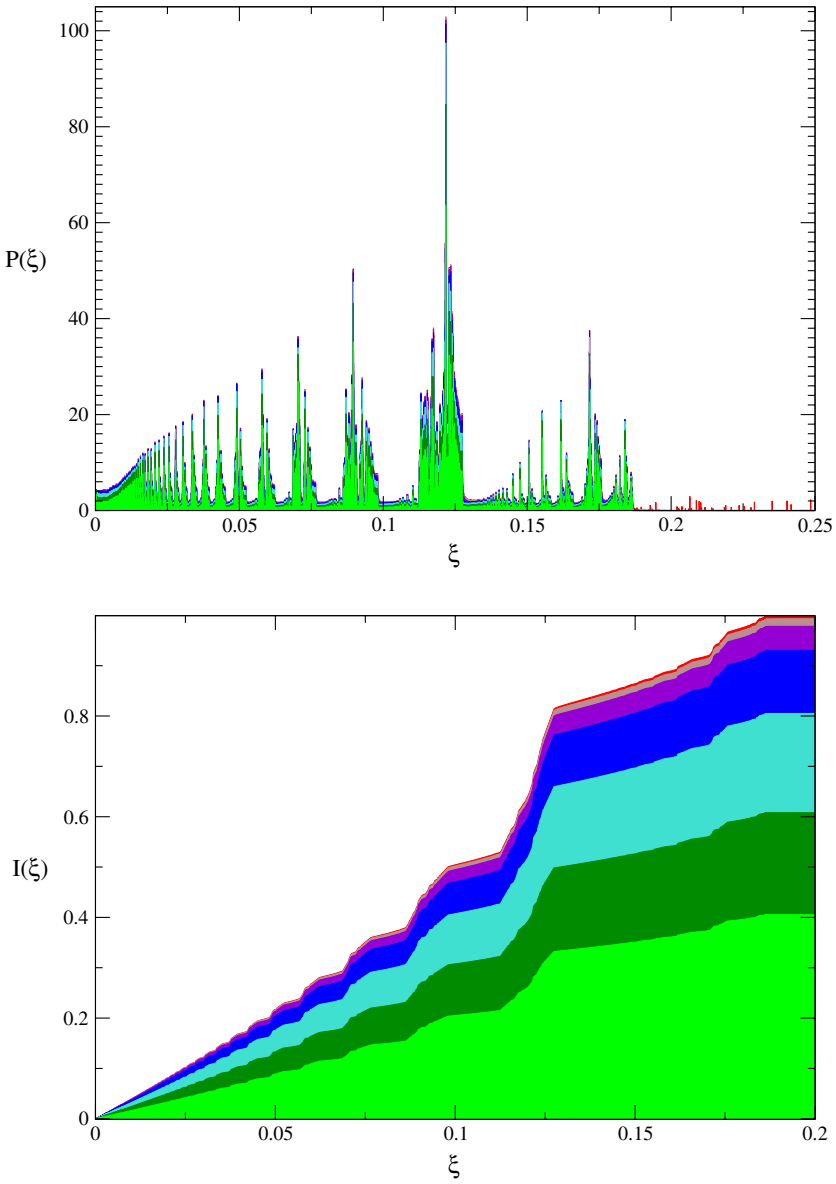

Figure 5. Upper panel: the nodal count distribution (histogram) for energies in the interval $9000^2 \leqslant \lambda_N \leqslant 2 \times 9000^2$. The colours (greyscales) represent the proportion of wavefunctions with no tiling behaviour (light green), with exactly 2 tiles (dark green), with 4–9 tiles (turquoise), with 10 to 99 tiles (blue), with 100–999 tiles (violet), with 1000–9999 tiles (grey) and with more than 10 000 tiles (red). Lower panel: the corresponding integrated nodal count distribution.

extensive number of nodal counts included we cannot be sure whether a limiting distribution exists. Still it is interesting to note that, in a certain sense, the asymptotic behaviour contains some features of chaotic systems. In a chaotic billiard, one sees a single peak which becomes a delta-function as $\lambda \to \infty$. For the isosceles triangle, we see a large number of peaks—and the numerics suggests that each one may converge to a delta-function. Another obvious question suggested by the numerics is whether the limiting distribution contains fractal features.

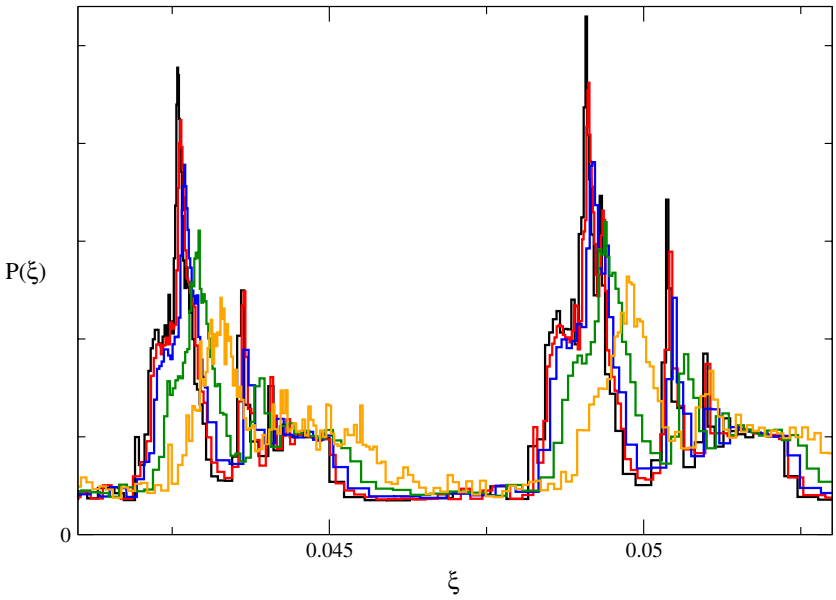

Figure 6. A detail of the nodal count distribution $P_{\lambda,1}(\xi)$ that shows the limiting behaviour. The five curves are histograms for $\lambda = 1000^2$ (orange), $\lambda = 2000^2$ (green), $\lambda = 4000^2$ (blue), $\lambda = 6000^2$ (red) and $\lambda = 9000^2$ (black).

3.2. The cumulative nodal loop count

We have already observed in section 2.4 that, at least for the non-tiling case, the nodal count decomposes to the number of boundary intersections and the nodal loop count (2.1). The number of boundary intersections for the triangle was already investigated in [28] and presented as a trace formula. In this section, we thus focus on the nodal loop count. Denoting by ι_n the nodal loop count of the nth eigenfunction, we define two cumulative continuous counting functions:

$$Q(N) := \sum_{n=1}^{\lfloor N \rfloor} \iota_n,$$
$$C(k) := \sum_{n=1}^{\infty} \iota_n \Theta(k - k_n),$$

where $\lfloor N \rfloor$ denotes the largest integer smaller than N, k_n is the square root of the nth eigenvalue (multiple eigenvalues appear more than once in the sequence $\{k_n\}$) and $\Theta(k)$ is the Heaviside theta function. It should be noted that the functions above can be obtained one from the other by the use of the spectral counting function, $N(k) = \sum_{n=1}^{\infty} \Theta(k - k_n)$, or its inversion. Previous works examined similar nodal counting functions for separable drums [23, 24]. It was proved that for simple tori and surfaces of revolution the nodal counting function can be presented as a trace formula. The counting function was expressed there as a sum of two parts: a smooth (Weyl) term which reflects the global geometrical parameters of the drum and an oscillating term which depends on the lengths of the classical periodic orbits on the drum. For example,

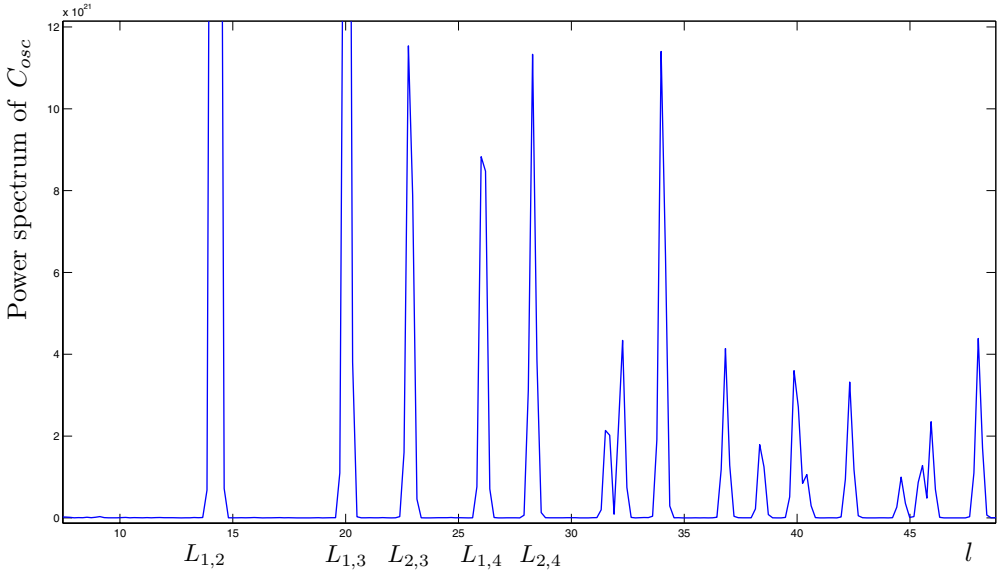

Figure 7. The power spectrum of $C_{\rm osc}\,(k)$. The lengths of some periodic orbits are identified on the l axis.

it was shown in [23, 24] that the smooth part of $\sum_{n=1}^{\lfloor N\rfloor}\nu_n$ is $\mathrm{O}(N^2)$, and the oscillating term has the form

$$N^{\frac{5}{4}}\sum_{\rm po}a_{\rm po}\sin\left(L_{\rm po}\sqrt{\frac{4\pi}{A}N}+\varphi_{\rm po}\right),$$

where the sum is over the periodic orbits, $L_{\rm po}$ is the length of the orbit, $a_{\rm po}$ and $\varphi_{\rm po}$ are some coefficients, which depend on the orbit, and A is the total area of the drum. Results for other separable drums have the same form.

Having in mind the case of separable drums, we have examined both $Q\,(N)$ and $C\,(k)$ numerically and found that both counting functions have a (numerically) well-defined smooth term and an oscillatory term. Like in the case of the separable drums, the smooth term of $C\,(k)$ was found to be $\mathrm{O}(k^4)$ as well. Note that the accumulated boundary intersections count $\sum_{n=1}^{\infty}\eta_n\Theta\,(k-k_n)$ is only $\mathrm{O}(k^3)$. Hence, for high-energy eigenfunctions, most of the nodal domains do not touch the boundary. We have extracted the oscillatory part by numerically interpolating the smooth term and then subtracting it from $C\,(k)$. In order to reveal whether periodic orbits contribute in a similar way as in the separable case, we evaluated the Fourier transform of the oscillatory term $C_{\rm osc}\,(k)$. The result is shown in figure 7 where the transform was performed for the interval

$$(k_{62\,439\,153},\,k_{62\,831\,853})\approx(\sqrt{9466^2+8332^2},\,\sqrt{10\,046^2+7688^2}).$$

The Fourier transform in figure 7 shows clear peaks at positions which correspond to lengths of periodic orbits in the triangle. For each value of $(p,q)\in\mathbb{Z}^2\setminus\{(0,0)\}$, there exists a continuous family of orbits of length $L_{p,q}=2\pi\sqrt{p^2+q^2}$. These are orbits that bounce from the bottom cathetus ($y=0$) at an angle of $\arctan(q/p)$.

The investigation of $Q\,(N)$ starts similarly by extracting its oscillating part. As can be expected from Weyl's formula, the smooth part is $\mathrm{O}(N^2)$. However, the Fourier transform of $Q_{\rm osc}\,(N)$ should be done with respect to a scaled variable rather than N. For this purpose, we

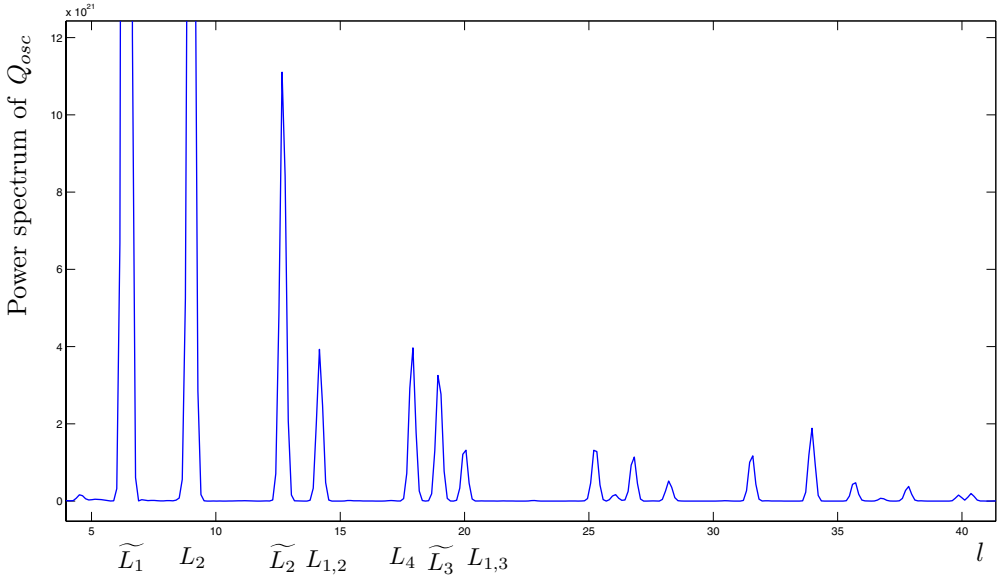

Figure 8. The power spectrum of $Q_{\rm osc}\,(q)$. The lengths of some periodic orbits are identified on the l axis.

use the Weyl term of the counting function, $N \approx \frac{A}{4\pi}\lambda_N$, where $A = \frac{1}{2}\pi^2$ is the area of $\mathcal{D}$ and λ_N is the nth eigenvalue. The scaled variable used for the Fourier transform is the square root of the Weyl-estimated eigenvalue, $q \equiv \sqrt{\frac{4\pi}{A}N} = \sqrt{\frac{8}{\pi}N}$. Fourier transforming $Q_{\rm osc}$ with respect to q, reveals a linear combination of delta-like peaks. The positions of these peaks reproduce the lengths of some of the periodic orbits mentioned above and of some additional ones.

(1) Isolated orbits that hit the corner $(\pi, 0)$ at 45°. The length of such orbits is $L_n = \sqrt{2}\pi n$, where $n \in \mathbb{N}$ is the number of repetitions of the basic orbit.
(2) Isolated orbits that go along one of the catheti. Their length is $\tilde{L}_n = 2\pi n$, where $n \in \mathbb{N}$ is the number of repetitions of the basic orbit.

Figure 8 shows the power spectrum of $Q_{\rm osc}(q)$, done when analysing $Q(N)$ in the interval $N \in (38\,877\,209, 39\,269\,906)$.

The above numeric investigation suggests a few observations. The clean Fourier transforms of both $C_{\rm osc}$ and $Q_{\rm osc}$ indicate on the existence of a trace formula for both. The need to rescale the variable before Fourier transforming $Q_{\rm osc}$ suggests that the source of a trace formula for $Q\,(N)$ is the trace formula of $C\,(k)$ combined with the inversion of the spectral counting function, $N\,(k)$. A similar relation between the boundary intersections counting functions was revealed in [28]. Another observation is that only the continuous families of periodic orbits appear in the Fourier transform of $C_{\rm osc}$. This is fundamentally different from the trace formula of the boundary intersections ([28]) and calls for further investigation. We suggest that the isolated periodic orbits which do appear in the Fourier transform of $Q_{\rm osc}$ are caused by the spectral inversion.

4. Summary and discussion

This paper investigates the nodal set of the Laplacian eigenfunctions of the right-angled isosceles triangle. The novelty of the work is the ability to obtain exact results for the nodal

count, although this problem is not separable. The algorithm described in section 2.3 constructs a graph which reflects the topology of the nodal set of a given eigenfunction. The graph contains complete and exact information about various properties of the nodal set (such as the number of nodal loops and the number of nodal domains) which can be calculated straightforwardly. The standard algorithm used for computing the number of nodal domains for a known (non-separable) eigenfunction on a drum is the Hoshen–Kopelman algorithm [10]. It samples the eigenfunction on a grid of finite resolution. As far as we know all implementations of the Hoshen–Kopelman algorithm for nodal counting use a fixed grid and calculate the number of nodal domains as an approximation. In principle, one may reduce the error by increasing the resolution of the grid near avoided crossing. However, the application of this algorithm assumes *a priori* that there are no nodal intersections. For the special algorithm we provide here we have proven that it gives the exact result, even though it samples the eigenfunction more sparsely than the Hoshen–Kopelman. This also leads to a somewhat faster running time of our algorithm (for both algorithms the running time is proportional to the energy λ—however the constant of proportionality is lower for our algorithm).

Our result may be generalized to other domains where similar algorithms may apply. Our algorithm is based on the fact that the eigenfunctions are presented as a linear combination of simple plane waves. It is therefore tempting to try and generalize it for other drums with similar property. The equilateral triangle is an immediate candidate (see [29] and references within).

A further, and quite surprising, result is the recursive formula for the number of nodal loops. To our knowledge this is the first known exact formula for the nodal count of a non-separable planar manifold (for certain eigenfunctions of tori exact formulas have been given in [22]). The formula was found by direct inspection of large tables and has been verified for a large bulk of data computationally. An obvious challenge is to prove this formula. In particular, the recursive part of the formula resembles the famous Euclid algorithm for the greatest common divisor. A further investigation of the mentioned formula might therefore expose some new number theoretical properties of the nodal count.

The recursive formula enables us to compute a large amount of data and to study the statistical properties of the nodal count sequence. We have studied this sequence using functions which are commonly used in research of nodal domains: the nodal count distribution and the cumulative nodal count. The nodal count distribution showed an intriguing structure that resembles neither the behaviour known from separable billiards nor the one of chaotic billiards. If at all, there is some similarities to the chaotic case, where the limiting distribution is a single delta function, whereas in our case it contains a large number of peaks.

In our analysis of the cumulative nodal count, we found numerical evidence for the existence of a trace formula similar to the one recently derived for separable drums [23, 24]. An open question is therefore to prove the existence of a trace formula in our case, shedding more light on the question ‘can one count the shape of a drum?’.

Acknowledgments

We are grateful to Uzy Smilansky for presenting the problem with us and for continuous support of the work. We thank Amit Godel for fruitful discussions. AA and RB thank the University of Nottingham for hospitality. DF and SG thank the Weizmann Institute for hospitality. The work was supported by ISF grant 169/09. RB is supported by EPSRC, grant no EP/H028803/1. DF was supported by the Minerva Foundation.

Appendix. Proofs of three lemmas

Lemma A.1. *Let*

$$\varphi_{m,n}(x,y) = \sin(mx)\sin(ny) - \sin(nx)\sin(my), \tag{A.1}$$

be an eigenfunction of the Laplacian on $\mathcal{D}$, where m and n obey $\gcd(m,n) = (m+n) \bmod 2 = 1$. *Then, there are no crossings of the nodal set of $\varphi_{m,n}$ in the interior of $\mathcal{D}$.*

Proof. The necessary conditions for a crossing to happen at a point (x, y) are

$$\begin{aligned}\varphi_{m,n}(x,y) &= 0,\\ \nabla\varphi_{m,n}(x,y) &= 0.\end{aligned}$$

After some algebraic manipulations the equations above obtain

$$\frac{\sin(nx)}{\sin(mx)} = \frac{\sin(ny)}{\sin(my)}, \tag{A.2}$$

$$\frac{\tan(nx)}{\tan(mx)} = \frac{n}{m}, \tag{A.3}$$

$$\frac{\tan(ny)}{\tan(my)} = \frac{n}{m}. \tag{A.4}$$

Combining (A.2) , (A.3) and (A.4) gives

$$\frac{\cos(nx)}{\cos(mx)} = \frac{\cos(ny)}{\cos(my)}.$$

Squaring this and using (A.2) allows us to conclude that one of the following holds:

$$\begin{aligned}\sin^2(my) &= \sin^2(ny) \text{ or}\\ \sin^2(my) &= \sin^2(mx).\end{aligned}$$

Assuming $\sin^2(my) = \sin^2(ny)$ immediately leads to $\frac{n}{m} = \pm 1$, which contradicts the assumptions on the values of m and n. Assuming $\sin^2(my) = \sin^2(mx)$ leads to $\sin^2(ny) = \sin^2(nx)$. We are now required to examine several possibilities for the relations of the expressions mx, my, nx, ny. Such an examination shows that each possibility will lead to a contradiction with the requirements $x, y \in (0, \pi)$ and the conditions $\gcd(m,n) = (m+n) \bmod 2 = 1$. □

From now on we consider only m, n obeying the non-tiling conditions. Recall the following definitions. Let φ_{mn} be an eigenfunction of the form (A.1) and

$$\begin{aligned}\varphi^1_{mn}(x) &= \sin(mx)\sin(ny)\\ \varphi^2_{mn}(x) &= \sin(nx)\sin(my).\end{aligned}$$

Furthermore,

$$\begin{aligned}N^1_{m,n} &= \left\{(x,y)\in\mathcal{D}\middle| x\in\frac{\pi}{m}\mathbb{N}\vee y\in\frac{\pi}{n}\mathbb{N}\right\},\\ N^2_{m,n} &= \left\{(x,y)\in\mathcal{D}\middle| x\in\frac{\pi}{n}\mathbb{N}\vee y\in\frac{\pi}{m}\mathbb{N}\right\} \quad \text{and}\\ V_{m,n} &= \left\{\frac{\pi}{m}(i,j)|0<j<i<m\right\}\cup\left\{\frac{\pi}{n}(i,j)|0<j<i<n\right\}.\end{aligned}$$

By $\mathcal{N}(\varphi_{mn})$ we denote the nodal set of φ_{mn}. Let $\mathcal{I}_c \subset \mathcal{D}\setminus(N^1_{m,n}\cup N^2_{m,n})$ be a rectangular shaped cell whose boundary is contained in $N^1_{m,n}\cup N^2_{m,n}$ and contains c points from $V_{m,n}$, with p_0 being its centre point. We also assume that $\forall(x,y)\in\mathcal{I}_c : \operatorname{Sign}\varphi^1_{mn}(x,y) = \operatorname{Sign}\varphi^2_{mn}(x,y)$.

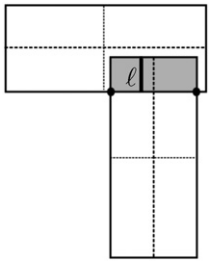

Figure A1. Example of a superposition of the nodal pattern of φ^1 and φ^2.

Lemma A.2.

(i) $\mathcal{N}(\varphi_{mn}) \cap \mathcal{I}_2$ *consists of a non-self-intersecting line connecting the nodal corners of* $\mathcal{I}_2$.
(ii) $\pm\varphi_{mn}(p_0) > 0$ *and* $\mathcal{N}(\varphi_{mn}) \cap \mathcal{I}_4$ *consists of two separated lines each connecting adjacent nodal corners along edges with* $\mp\varphi_{mn} > 0$.

Proof. Nodal sets on two-dimensional manifolds are submanifolds except for a closed set of lower dimension, where nodal lines intersect. For an eigenfunction φ_{mn} this singular set is characterized by $\varphi_{mn}^{-1}(0) \cap (\nabla\varphi_{mn})^{-1}(0)$. The boundary of a rectangle $\mathcal{I}_2$ with two points of V_{mn} intersects the nodal set only at those two points. By elementary arguments using the monotonicity of the sin function, the existence of nodal lines that do not intersect with the boundary of this rectangle can be ruled out. The nodal set has to connect the nodal corners, since nodal lines do not end. We present this argument in detail for one specific case and leave the other cases to the reader. We consider the situation of figure A1.

Let the rectangle $\mathcal{I}_2$ be in this case such that only one symmetry axis of the two nodal domains of φ_{mn}^1 and φ_{mn}^2 enters $\mathcal{I}_2$. The symmetry axes are the dotted lines and $\mathcal{I}_2$ is shaded. The vertices on the lower corners belong to the nodal set and the boundary of $\mathcal{I}_2$ between those two points belongs to a nodal domain of φ_{mn} with positive sign (assume this for now—for negative sign it would be the same argument). Then, the upper boundary of $\mathcal{I}_2$ belongs to a nodal domain of φ_{mn} with a negative sign. We study now the behaviour of φ on a vertical line ℓ between the upper and lower boundaries—like the one displayed in the figure. Note first that the horizontal rectangle in the figure is a nodal domain of φ_{mn}^2 with a positive sign, while the vertical rectangle is a nodal domain of φ_{mn}^1 with a positive sign. On the lower end of ℓ, φ_{mn}^2 starts when its value is equal to zero and grows strictly monotonic on ℓ until it reaches the boundary at a positive value. φ_{mn}^1 starts with a positive value and falls strictly monotonic ending at zero. φ_{mn} being the difference of φ_{mn}^1 and φ_{mn}^2 equals zero exactly once on ℓ. This is true for any ℓ. The nodal set therefore intersects every ℓ exactly once and therefore has no intersections nor further isolated nodal domains.
In the case of rectangles with four points of V_{mn}, there is a line of constant sign of φ_{mn} running through the centre, which cannot be intersected by a nodal line. It can be concluded as above that the nodal corners are joined by nodal lines within the two remaining components of this rectangle. □

Let $\mathcal{T} \subset \mathcal{D} \setminus (N_{m,n}^1 \cup N_{m,n}^2)$ be a triangular shaped cell next to the boundary with $\operatorname{Sign}\varphi_{mn}^1(x, y) = \operatorname{Sign}\varphi_{mn}^2(x, y)$ in $\mathcal{T}$. Let $\mathcal{I}^b \subset \mathcal{D} \setminus (N_{m,n}^1 \cup N_{m,n}^2)$ be a rectangular shaped cell next to the boundary with $\operatorname{Sign}\varphi_{mn}^1(x, y) = \operatorname{Sign}\varphi_{mn}^2(x, y)$ in $\mathcal{I}^b$.

Lemma A.3.

(i) A triangular cell $\mathcal{T}$ contains a nodal line iff $\overline{\mathcal{T}}$ contains a point of $V_{m,n}$. $\mathcal{N}(\varphi_{mn}) \cap \mathcal{T}$ is a nodal line connecting this point to the boundary.

(ii) If $\overline{\mathcal{I}^b}$ contains one point of $V_{m,n}$ then $\mathcal{N}(\varphi_{mn}) \cap \mathcal{I}^b$ is a nodal line connecting this point to the boundary.

(iii) If $\overline{\mathcal{I}^b}$ contains two points of $V_{m,n}$ then $\mathcal{N}(\varphi_{mn}) \cap \mathcal{I}^b$ is a nodal line connecting those two points.

Proof. In order to understand the run of the nodal set, the nodal pattern is continued beyond the hypotenuse by defining the eigenfunction on the whole square to be the continuation of the eigenfunction on the triangle. This rectangle can now be treated just as in lemma A.2 with two points of $V_{m,n}$ on the left -lower and right-upper corners. The resulting nodal line coincides with the hypotenuse. In case there is a point of $V_{m,n}$ on the right-lower corner, there is also one in the left-upper corner by symmetry and the case with four nodal corners from lemma A.2 applies, and shows the existence of a nodal line connecting the right lower corner with the boundary. The other points are proven similarly to the proof of lemma A.2 by monotonicity of φ^1 and φ^2. □

References

[1] Chladni E F F 1802 *Die Akustik* (Leipzig: Breitkopf and Härtel)

[2] Sturm J C F 1836 Sur les équations différentielles linéaires du second ordre *J. Math. Pures Appl. Liouville* **1** 106–86
Sturm J C F 1836 Sur une classe d'équations différentielles partielles *J. Math. Pures Appl. Liouville* **1** 375–444

[3] Courant R 1923 Ein allgemeiner Satz zur Theorie der Eigenfunktionen selbstadjungierter Differentialausdrücke *Nachrichten von der Gesellschaft der Wissenschaften zu Göttingen, Mathematisch-Physikalische Klasse (Göttingen, 13 July 1923)* pp 81–4

[4] Blum G, Gnutzmann S and Smilansky U 2002 Nodal domain statistics: a criterion for quantum chaos *Phys. Rev. Lett.* **88** 114101

[5] Keating J P, Mezzadri F and Monastra A G 2003 Nodal domain distributions for quantum maps *J. Phys. A: Math. Gen.* **36** L53

[6] Savytskyy N, Hul O and Sirko L 2004 Experimental investigation of nodal domains in the chaotic microwave rough billiard *Phys. Rev.* E **70** 056209

[7] Hul O, Savytskyy N, Tymoshchuk O, Bauch S and Sirko L 2005 Investigation of nodal domains in the chaotic microwave ray-splitting rough billiard *Phys. Rev.* E **72** 066212

[8] Aiba H and Suzuki T 2005 Nodal domain distribution for a nonintegrable two-dimensional anharmonic oscillator *Phys. Rev.* E **72** 066214

[9] Smilansky U and Sankaranarayanan R 2005 Nodal domain distribution of rectangular drums *Proc. Natl. Conf. on Nonlinear Systems and Dynamics (Aligarh Muslim University, India, 24–26 Feb. 2005)*

[10] Hoshen J and Kopelman R 2006 Percolation and cluster distribution: I. Cluster multiple labeling technique and critical concetntration algorithm *Phys. Rev.* B **14** 3438

[11] Monastra A G, Smilansky U and Gnutzmann S 2003 Avoided intersections of nodal lines *J. Phys. A: Math. Gen.* **36** 1845

[12] Berry M V 1977 Regular and irregular semiclassical wave functions *J. Phys. A: Math. Gen.* **10** 2083

[13] Bogomolny E and Schmit C 2002 Percolation model for nodal domains of chaotic wave functions *Phys. Rev. Lett.* **88** 114102

[14] Foltin G, Gnutzmann S and Smilansky U 2004 The morphology of nodal lines random waves versus percolation *J. Phys. A: Math. Gen.* **37** 11363

[15] Bogomolny E and Schmit C 2007 Random wavefunctions and percolation *J. Phys. A: Math. Theor.* **40** 14033

[16] Keating J P, Marklof J and Williams I G 2006 Nodal domain statistics for quantum maps, percolation and SLE *Phys. Rev. Lett.* **97** 034101

[17] Bogomolny E, Dubertrand R and Schmit C 2007 SLE description of the nodal lines of random wave functions *J. Phys. A: Math. Theor.* **40** 381

[18] Keating J P, Marklof J and Williams I G 2008 Nodal domain statistics for quantum chaotic maps *New J. Phys.* **10** 083023
[19] Nazarov F and Sodin M 2009 On the number of nodal domains of random spherical harmonics *Am. J. Math.* **131** 1337
[20] Gnutzmann S, Smilansky U and Søndergaard N 2005 Resolving isospectral drums by counting nodal domains *J. Phys. A: Math. Gen.* **38** 8921
[21] Brüning J, Klawonn D and Puhle C 2007 Comment on 'Resolving isospectral drums by counting nodal domains' *J. Phys. A: Math. Theor.* **40** 15143
[22] Brüning J and Fajman D 2012 On the nodal count for flat tori *Commun. Math. Phys.* at press
[23] Gnutzmann S, Karageorge P and Smilansky U 2006 Can one count the shape of a drum? *Phys. Rev. Lett.* **97** 090201
[24] Gnutzmann S, Karageorge P and Smilansky U 2007 A trace formula for the nodal count sequence—towards counting the shape of separable drums *Eur. Phys. J. Spec. Top.* **145** 217
[25] Karageorge P D and Smilansky U 2008 Counting nodal domains on surfaces of revolution *J. Phys. A: Math. Theor.* **41** 205102
[26] Klawonn D 2009 Inverse nodal problems *J. Phys. A: Math. Theor.* **42** 175209
[27] Pleijel A 1956 Remarks on Courant's nodal line theorem *Commun. Pure Appl. Math.* **9** 543
[28] Aronovitch A and Smilansky U 2012 Nodal domains on boundaries of 2D billiards (in preparation)
[29] McCartin B J 2003 Eigenstructure of the equilateral triangle: part I. The Dirichlet problem *SIAM Rev.* **45** 267